11th World Congress on Computational Mechanics (WCCM XI)
5th European Conference on Computational Mechanics (ECCM V)
6th European Conference on Computational Fluid Dynamics (ECFD VI)
E. Oñate, J. Oliver and A. Huerta (Eds)

ON MODELING THREE-COMPONENT POROUS MEDIA INCORPORATING HYSTERESIS

BETTINA ALBERS

Technische Universität Berlin
Department of Soil Mechanics and Geotechnical Engineering
Sekr. TIB1-B7, Gustav-Meyer-Allee 25, 13355 Berlin, Germany
e-mail: albers@grundbau.tu-berlin.de, web page: www.mech-albers.de

Key words: Partially saturated porous media, Hysteresis, Capillary pressure, Application to wave propagation

Abstract. Final aim is to find a closed-form model including a hysteresis operator to describe wave propagation processes in partially saturated soils. Two models which not completely fulfil this goal are presented in this paper. The first is a mathematical soil-moisture hysteresis model in which the Preisach operator is used. However, this model by Flynn [5] is parabolic and thus, is not suitable to describe wave propagation. The other is a hyperbolic but linear model which does not include an operator to describe hysteresis [3]. Nevertheless, hysteresis is accounted for: the wave analysis is performed for the two limit cases of main drying and main wetting. As in [2] the influence of the application of drying and wetting data on the propagation of sound waves is studied for the example of Del Monte sand filled by an air-water mixture. Four waves appear: one transversal wave and three longitudinal waves. For the waves driven mainly by the skeleton it could be expected that the influence of the hysteresis in the capillary pressure curve is negligible. This is different from the expectations for the waves driven by the pore fluids. The numerical results exhibit – at least for the present example – a smaller influence than expected.

1 INTRODUCTION

If the pores of a porous medium are filled by two (or more) immiscible fluids, as for example, water and air, then they are called 'partially saturated'. The pore fluids possess different partial pressures, i.e. a discontinuity exists in the pressure across the interface separating them. This difference is called capillary pressure p_c. It depends on the geometry of the pore space, on the nature of the solids and on the degree of saturation S, i.e. the ratio of the volume occupied by one of the pore fluids over the entire pore volume. The capillary pressure exhibits different values depending on the initial state of saturation. If,

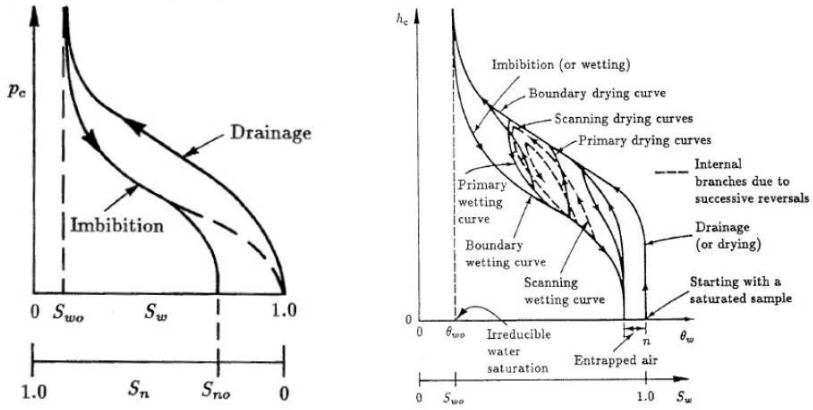

Figure 1: Hysteresis in capillary pressure curves. Left: one cycle, right: three cycles (taken from Bear & Bachmat [4])

initially, a sample is saturated by a wetting fluid then drainage takes place. In the case of a non-wetting fluid filling the pore space initially, the wetting fluid tends to spread on the solid wall by imbibition (wetting), gradually displacing the non-wetting fluid. The hysteresis, i.e. the occurrence of two different branches of the capillary pressure curve as function of the saturation, reflects the dependence of the curve upon the history of draining and wetting (see left panel of Figure 1).

For simplicity, in most approaches of partially saturated porous media – including my own investigations (see: [3]) – only one of the branches is taken into account. But also models including hysteresis exist. General thoughts concerning hysteresis, following from studies of magnetism or ferroelectrics, have been taken into account in modeling soil-moisture hysteresis. The outcome are several either empirical or mathematically derived models which are introduced in details in [1].

Both empirical models and mathematical approaches aim to fit experimental results as accurately as possible. Often, not only values on the main hysteresis curves (boundary curves) but also on inner hysteresis curves (so-called scanning curves) which occur upon re-wetting and re-drying (see right panel of Figure 1) are of interest. Because of big differences in the capillary pressure for different degrees of saturation the measurement is labourious and time consuming and often application of more than one method is necessary. Of course, one strives to perform as little measurements as possible and to predict the properties of the curves theoretically.

2 EXAMPLE FOR A PARABOLIC MODEL OF SOIL-MOISTURE HYSTERESIS USING THE PREISACH OPERATOR

The first approach introduced here is a mathematical treatment of soil-moisture hysteresis based on the Preisach model.

After Flynn [5] the standard approach to the mathematical treatment of hysteresis has

the following structure: 1) to choose an elementary rate independent hysteresis nonlinearity, a so called hysteron; 2) to treat the complex rate independent hysteresis nonlinearities as block-diagrams of hysterons and 3) to establish identification principles.

One frequently used type of hysteron is the non-ideal relay – it is the basic idea of the Preisach model [11]. It is characterized by its threshold values $\alpha < \beta$ and internal memory state $\eta(t)$. Its output can take one of the two values 0 or 1 which means that at any moment the relay is either 'switched off' or 'switched on'. The output $y(t) = R_{\alpha,\beta}[t_0, \eta_0]\, x(t)$, depends on the input $x(t)$ and on the initial state η_0 which is either 0 or 1. The main assumption made in the Preisach model is that the system can be thought of as a parallel summation of a continuum of weighted non-ideal relays $R_{\alpha,\beta}$, where the weighting of each relay is $\mu(\alpha, \beta)$. Such a summation can be uniquely represented as a collection of non-ideal relays as points on the two-dimensional half-plane $\Pi = \{(\alpha, \beta) : \beta > \alpha\}$, which is also known as the Preisach plane (the neighboring figure shows an illustration by Flynn [5]). The colored area $S = S(t)$ is the set of the threshold values (α, β) for which the corresponding relays $R_{\alpha,\beta}$ are in the 'on' state at a given moment t. $L(t)$ (the so called staircase) is the interface between the relays, $R_{\alpha,\beta}$, which are in the 'on' or 'off' states. The output of the Preisach model is then represented by the following formula:

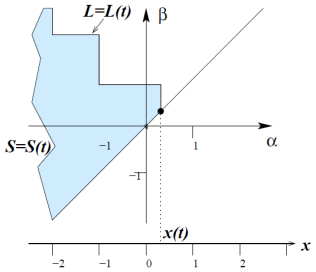

Figure 2: Typical state of a Preisach plane (from [5]).

$$y(t) = \int_{\alpha<\beta} p(\alpha, \beta)\, R_{\alpha,\beta}[t_0, \eta_0(\alpha, \beta)]\, x(t)\, d\alpha d\beta = \int_{S(t)} p(\alpha, \beta)\, d\alpha d\beta, \tag{1}$$

where $p(\alpha, \beta)$ is an integrable positive function in Π. This function is also called the Preisach density. Flynn in [5] studies a family of ordinary differential equations with Preisach hysteresis. He calls them hysteretic differential equations (HDEs) and uses them to describe the flow of liquids through porous media. In the following the model will be presented: First the mass balance equation is considered

$$\rho_w \dot{\theta} = \rho_w q, \quad \theta(0) = \theta_0, \quad 0 \le \theta \le \theta_s < 1, \tag{2}$$

where ρ_w is the density of water (obviously, for the case of uniform density of water ρ_w can be canceled out), $\dot{\theta} = \frac{d\theta}{dt}$, θ_s is the moisture content at natural saturation and q is the net inflow rate of water volume per unit time into a representative elementary volume (REV). It is assumed that the moisture content is related to the matric potential ψ by the Preisach operator, i.e. $\theta(\psi) = P(\psi)$. Thus, hysteresis enters equation (2) which becomes the following HDE

$$\frac{dP[\psi]}{dt} = q, \quad \theta(0) = \theta_0, \quad 0 \le \theta \le \theta_s < 1. \tag{3}$$

In order to close this equation, a law is needed, relating the rate of the liquid flow through the porous medium to the potential difference, i.e. to Darcy's law. This law states that

the flow past two points in the medium is proportional to the difference in their potentials (ψ_1 and ψ_2), and is inversely proportional to the distance, L, between them

$$q \propto \frac{\psi_1 - \psi_2}{L}. \tag{4}$$

For simplicity, Flynn sets $L = 1$ m and expresses the law as an equation using the proportionality constant k_c, the conductivity term. Finally, the simplified Darcy law is

$$q = k_c \left(\psi_1 - \psi_2\right). \tag{5}$$

If now one of the potentials is considered as a reference potential, the HDE for the hydrological model takes the following form

$$\frac{d\mathcal{P}\left[\psi\right]}{dt} = f\left(t, \psi\right) = k_c \left(\psi - \psi_{ref}\right), \tag{6}$$

where $\mathcal{P}$ is the Preisach operator.

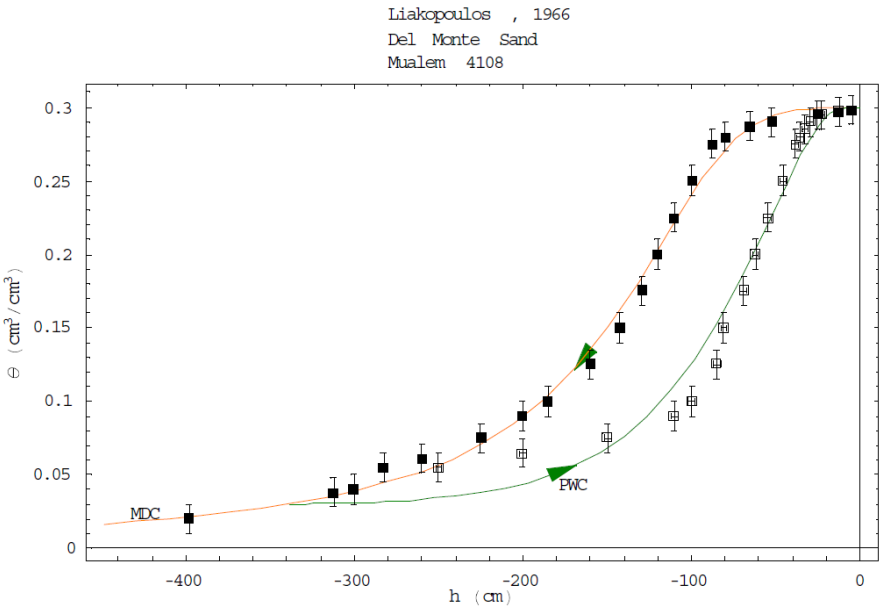

Figure 3: Data sets of Del Monte sand (from [7]) and fit by use of the 'Wedge Model' by Flynn [5].

In the book chapter of Flynn et al. [6] and in his Phd thesis [5] three different types of Preisach densities are investigated and compared, here, only one is picked. It is called the 'Wedge model' and the classical van Genuchten equation for the main drying curve is used to determine the main wetting and the scanning curves

$$\theta\left(\psi\right) = \theta_r + \left(\theta_s - \theta_r\right)\left[1 + \left(\frac{h}{h_g}\right)^n\right]^{-m}, \tag{7}$$

therein θ is the volumetric water content, θ_r the residual water content, θ_s the water content at natural saturation, h the soil water pressure head or matric potential, h_g a van Genuchten pressure head scale parameter and n and m are van Genuchten shape parameters. The 'Wedge model' contains a one-parameter density, distributed between the line $\beta = \alpha$ and the line $\beta = \gamma\alpha$, where $0 \leq \gamma \leq 1$ is the parameter of the model. The density within this range is given by

$$p_\gamma(\alpha, \beta) = \frac{\theta_s}{\alpha(1-\gamma)} \frac{d}{d\alpha} \left(1 + \left(\frac{\alpha}{h_g}\right)^n\right)^{-m}. \tag{8}$$

For the 'Wedge model' and each of the other models Flynn required some means of finding the best possible parameter value to fit the data. He used experimental data given in [7] for 21 soil types. The theoretical predictions fit well the experimental curves. In Figure 3 the fit for Del Monte sand, which is studied also further in this paper, is reproduced from [5].

3 LINEAR HYPERBOLIC MODELING OF SOIL-MOISTURE HYSTERESIS AND APPLICATION TO WAVE PROPAGATION

3.1 Main curves

Most hysteresis models for soils presented in the literature (on modeling hysteresis see e.g. [1]) presume that both the main drying curve (MDC) and the main wetting curve (MWC) (or alternatively the primary wetting curve (PWC) as illustrated in Figure 3) are measured and interpolate scanning curves (i.e. inner curves for further drying and wetting processes) from the data of both curves. Parlange, on the contrary [10], presented an approach to predict the second boundary and scanning curves in between from only one boundary curve. Since the measurements are laborious and time consuming this offers advantages compared with other methods. An inconvenience of this model is that it imposes a wetting curve without an inflection point [7]. Additionally, for the original model no analytical solution applied to the van Genuchten equation could be found. However, Haverkamp et al. [7] introduced an extension which implies that all drying and wetting curves (regardless of the scanning order) have the shape of the van Genuchten equation [12] in normalized form (7): $\theta^* = \frac{\theta - \theta_r}{\theta_S - \theta_r} = \left[1 + \left(\frac{h}{h_g}\right)^n\right]^{-m}$.

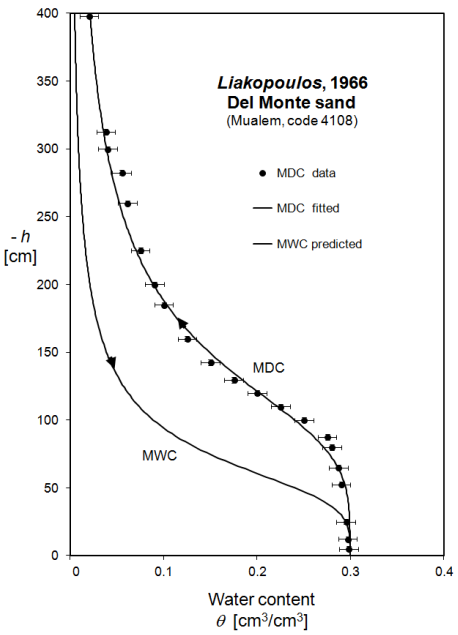

Figure 4: Main drying curve (MDC) fitted to measured drying data (•) for Del Monte sand taken from Liakopoulos 1966 [9]. The main wetting curve (MWC) has been predicted by [7].

The above mentioned postulation that all curves are expressed in form of the van Genuchten function leads to the following equations for the MWC and the MDC

$$\theta^*_{mw} \equiv \frac{\theta_{mw}}{\theta_{Smw}} = \left[1 + \left(\frac{h}{h_{gmw}}\right)^{n_{mw}}\right]^{-m_{mw}}, \quad \theta^*_{md} \equiv \frac{\theta_{md}}{\theta_{Smd}} = \left[1 + \left(\frac{h}{h_{gmd}}\right)^{n_{md}}\right]^{-m_{md}}, \quad (9)$$

where the subscripts mw and md refer to main wetting and main drying, respectively. Differently from the Parlange model these curves possess an inflection point. The relations between the specific wetting parameters m_{mw}, n_{mw} and h_{gmw} and the drying parameters m_{md}, n_{md} and h_{gmd} are specified in [7]

$$\begin{aligned} &m_{mw} = m_{md}, \\ &n_{mw} = n_{md}, \end{aligned} \qquad \text{and} \qquad h_{gmd} = 2h_{gmw}, \quad \text{for} \quad \begin{cases} m_{mw} n_{mw} \geq 1, \\ m_{md} n_{md} \geq 1. \end{cases} \quad (10)$$

The prediction of the primary wetting curve (PWC) from measured data has been demonstrated in [7] for 22 different soil samples. For each type the MDC has been fitted to experimental data, the MWC and PWC have been predicted theoretically and the latter curve been compared to measured data. In Figure 4 measured data of the MDC, the fitted MDC and the predicted MWC for Del Monte sand (originally presented in [9]) are reproduced. The resulting curves are used further to calculate the wave speeds and attenuations of the waves occuring in partially saturated Del Monte sand. The range of the acoustic properties is determined in calculating them for the limit cases: once the MDC, the other time the MWC is used representing the relation between capillary pressure and saturation.

3.2 Linear model for three-component materials

In [3] a linear model for three-component materials with an immiscible mixture of two pore fluids (F and G) in the pores of a solid material (S) has been introduced. The fields $\left\{\mathbf{v}^S, \mathbf{v}^F, \mathbf{v}^G, \mathbf{e}^S, \varepsilon^F, \varepsilon^G\right\}$, the velocities of the three components, the macroscopic deformation tensor $\mathbf{e}^S$ and the volume changes of fluid and gas, respectively, satisfy the following field equations

$$\begin{aligned} \rho_0^S \frac{\partial \mathbf{v}^S}{\partial t} &= \operatorname{div}\left\{\lambda^S e \mathbf{1} + 2\mu^S \mathbf{e}^S + Q^F \varepsilon^F \mathbf{1} + Q^G \varepsilon^G \mathbf{1}\right\} + \\ &\quad + \pi^{FS}\left(\mathbf{v}^F - \mathbf{v}^S\right) + \pi^{GS}\left(\mathbf{v}^G - \mathbf{v}^S\right), \\ \rho_0^F \frac{\partial \mathbf{v}^F}{\partial t} &= \operatorname{grad}\left\{\rho_0^F \kappa^F \varepsilon^F + Q^F e + Q^{FG} \varepsilon^G\right\} - \pi^{FS}\left(\mathbf{v}^F - \mathbf{v}^S\right), \\ \rho_0^G \frac{\partial \mathbf{v}^G}{\partial t} &= \operatorname{grad}\left\{\rho_0^G \kappa^G \varepsilon^G + Q^G e + Q^{FG} \varepsilon^F\right\} - \pi^{GS}\left(\mathbf{v}^G - \mathbf{v}^S\right), \\ \frac{\partial \mathbf{e}^S}{\partial t} &= \operatorname{sym}\operatorname{grad}\mathbf{v}^S, \quad \frac{\partial \varepsilon^F}{\partial t} = \operatorname{div}\mathbf{v}^F, \quad \frac{\partial \varepsilon^G}{\partial t} = \operatorname{div}\mathbf{v}^G, \quad e \equiv \operatorname{tr}\mathbf{e}^S. \end{aligned} \quad (11)$$

Instead of the partial mass densities of the components, ρ^S, ρ^F, ρ^G, the equations depend on the volume changes of the components $e, \varepsilon^F, \varepsilon^G$ which are defined by

$$e = \frac{\rho_0^S - \rho^S}{\rho_0^S}, \quad \varepsilon^F = \frac{\rho_0^F - \rho^F}{\rho_0^F}, \quad \varepsilon^G = \frac{\rho_0^G - \rho^G}{\rho_0^G}. \tag{12}$$

Quantities with subindex zero are initial values of the corresponding current quantities. Q^F, Q^G and Q^{FG} are coupling parameters between solid-fluid, solid-gas and fluid-gas, respectively. λ^S and μ^S are Lamé parameters. The compressibilities of fluid and gas are denoted by κ^F and κ^G.

In principle, the porosity n also is a field and satisfies an own balance equation. However, if we neglect memory effects, the balance equation can be solved and its consideration is not longer necessary to solve the problem. The current saturation of the fluid S is not included in the series of fields. Instead, a constitutive law of van Genuchten type will be used for this quantity.

The parameters π^{FS} and π^{GS} reflect relative resistances of the flow of the pore fluids through the channels of the skeleton. They are given by

$$\pi^{FS} = \frac{\pi^F}{k_f}, \qquad \pi^{GS} = \frac{\pi^G}{k_g}. \tag{13}$$

As obvious from Table 1, π^F and π^G account not only for the permeability of the solid but also for the viscosity of the pore fluid. Van Genuchten [12] not only proposed a theoretical relationship between the capillary pressure and the saturation but also formulae for the relative permeabilities k_f and k_g which depend on the degree of saturation

$$k_f = S^{\frac{1}{2}} \left[1 - \left(1 - S^{\frac{1}{m}}\right)^m\right]^2, \qquad k_g = (1-S)^{\frac{1}{3}} \left(1 - S^{\frac{1}{m}}\right)^{2m}. \tag{14}$$

The macroscopic material parameters $\left\{\lambda^S + \frac{2}{3}\mu^S, \kappa^F, \kappa^G, Q^F, Q^G, Q^{FG}\right\}$ appearing in (11) have to be specified according to the material. In [3] this is done by applying a transition from the micro- to the macro-scale. The capillary pressure/saturation relation proposed by van Genuchten is used. Instead of water contents and pressure head used as variables in (7) the relation is formulated for saturation and capillary pressure

$$p_c = \frac{1}{\alpha_{vG}} \left[S^{(-1/m_{vG})} - 1\right]^{1/n_{vG}}. \tag{15}$$

Therein parameters with index vG coincide with those without index quoted in Table 1. Applying the micro-macro transition both to the MDC and the MWC using the microscopic material parameters given in Table 1 leads to sets of macroscopic material parameters for main drying and main wetting.

3.3 Wave analysis – propagation of monochromatic waves

By means of the above introduced model the wave propagation in partially saturated soils is investigated. The fields of the model (11) are assumed to satisfy the relations

$$\varepsilon^F = E^F\mathcal{E}, \quad \varepsilon^G = E^G\mathcal{E}, \quad \mathbf{e}^S = \mathbf{E}^S\mathcal{E}, \quad \mathbf{v}^F = \mathbf{V}^F\mathcal{E}, \quad \mathbf{v}^G = \mathbf{V}^G\mathcal{E}, \quad \mathbf{v}^S = \mathbf{V}^S\mathcal{E},$$
$$n - n_0 = D\mathcal{E}, \qquad \mathcal{E} := \exp i\left(\mathbf{k}\cdot\mathbf{x} - \omega t\right), \tag{16}$$

where $\mathbf{E}^S, E^F, E^G, \mathbf{V}^S, \mathbf{V}^F, \mathbf{V}^G, D$ are constant amplitudes, ω is a given frequency and $\mathbf{k}$ is the wave vector. $\mathbf{k} = k\mathbf{n}$, where k is the complex wave number and $\mathbf{n}$ is a unit vector in the direction of propagation. Such a solution describes the propagation of plane monochromatic waves in an infinite medium whose fronts are perpendicular to $\mathbf{n}$.

Substitution of the above relations in the field equations $(11)_4$ yields the following compatibility relations

$$E^F = -\frac{1}{\omega}k\mathbf{n}\cdot\mathbf{V}^F, \quad E^G = -\frac{1}{\omega}k\mathbf{n}\cdot\mathbf{V}^G, \tag{17}$$
$$\mathbf{E}^S = -\frac{1}{2\omega}k\left(\mathbf{n}\otimes\mathbf{V}^S + \mathbf{V}^{\mathbf{S}}\otimes\mathbf{n}\right), \quad \text{i.e.} \quad e = -\frac{1}{\omega}k\mathbf{n}\cdot\mathbf{V}^S\mathcal{E}.$$

Making use of these relations in the remaining field equations leads to the following set

$$\begin{aligned}\omega^2\mathbf{V}^S = {}& \frac{\lambda^S}{\rho_0^S}k^2\left(\mathbf{V}^S\cdot\mathbf{n}\right)\mathbf{n} + \frac{\mu^S}{\rho_0^S}k^2\left(\left(\mathbf{V}^S\cdot\mathbf{n}\right)\mathbf{n} + \mathbf{V}^S\right) + \\ & + \frac{Q^F}{\rho_0^S}k^2\left(\mathbf{V}^F\cdot\mathbf{n}\right)\mathbf{n} + \frac{Q^G}{\rho_0^S}k^2\left(\mathbf{V}^G\cdot\mathbf{n}\right)\mathbf{n} + \\ & + i\frac{\pi^{FS}\omega}{\rho_0^S}\left(\mathbf{V}^F - \mathbf{V}^S\right) + i\frac{\pi^{GS}\omega}{\rho_0^S}\left(\mathbf{V}^G - \mathbf{V}^S\right) = 0,\end{aligned} \tag{18}$$

$$\begin{aligned}\omega^2\mathbf{V}^F = {}& \kappa^F k^2\left(\mathbf{V}^F\cdot\mathbf{n}\right)\mathbf{n} + \frac{Q^F}{\rho_0^F}k^2\left(\mathbf{V}^S\cdot\mathbf{n}\right)\mathbf{n} + \\ & + \frac{Q^{FG}}{\rho_0^F}k^2\left(\mathbf{V}^G\cdot\mathbf{n}\right)\mathbf{n} - i\frac{\pi^{FS}\omega}{\rho_0^F}\left(\mathbf{V}^F - \mathbf{V}^S\right) = 0,\end{aligned} \tag{19}$$

$$\begin{aligned}\omega^2\mathbf{V}^G = {}& \kappa^G k^2\left(\mathbf{V}^G\cdot\mathbf{n}\right)\mathbf{n} + \frac{Q^G}{\rho_0^G}k^2\left(\mathbf{V}^S\cdot\mathbf{n}\right)\mathbf{n} + \\ & + \frac{Q^{FG}}{\rho_0^G}k^2\left(\mathbf{V}^F\cdot\mathbf{n}\right)\mathbf{n} - i\frac{\pi^{GS}\omega}{\rho_0^G}\left(\mathbf{V}^G - \mathbf{V}^S\right) = 0.\end{aligned} \tag{20}$$

Separating the contributions and solving the eigenvalue problem yields dispersion relations for transversal and longitudinal waves. Their solutions specify both the phase velocities $c_{ph} = \frac{\omega}{\mathrm{Re}(k)}$ and the attenuations $\mathrm{Im}(k)$.

3.4 Numerical example: Del Monte sand filled by air and water

On the example of Del Monte sand filled by an air-water mixture the influence of the hysteresis in the capillary pressure curve on the propagation of sound waves is studied. This soil type has been chosen because the van Genuchten parameters needed for the

Table 1: Material properties of Del Monte sand filled by an air-water mixture.

real compressibility grains	$K_s = 35$ GPa
real compressibility fluid	$K_f = 2.25$ GPa
real compressibility gas	$K_s = 0.101$ MPa
Poisson's ratio	$\nu = 0.4$
shear modulus	$\mu^S = 0.85$ GPa
solid grain density	$\rho^{SR} = 2000$ kg m^{-3}
fluid density	$\rho^{FR} = 1000$ kg m^{-3}
initial porosity	$n_0 = 0.2975$
intrinsic permeability	$k = 4.5{\cdot}10^{-13}$ m^2
water conductivity	$\mathrm{K} = k\frac{\rho^{FR} g}{\mu_w} = 4.44{\cdot}10^{-6}$ m/s
water resistance	$\pi^F = \frac{n_0 \rho^{FR} g}{\mathrm{K}} = 6.573 \cdot 10^8$ kg m^{-3}s^{-1}
air resistance	$\pi^G = 1.82 \cdot 10^5$ kg m^{-3}s^{-1}
water viscosity	$\mu_w = 1{\cdot}10^{-3}$ Pa s
air viscosity	$\mu_a = 1.82{\cdot}10^{-5}$ Pa s
van Genuchten parameter	$n = 4.150$ $m = 0.518$
h_g for drying and wetting	$h_{gd} = 116.56$ cm $h_{gw} = 58.28$ cm
α for drying and wetting	$\alpha_d = 8.745 \cdot 10^{-5}$ Pa $\alpha_w = 1.749 \cdot 10^{-4}$ Pa
earth acceleration	$g = 9.81$m s^{-2}

pressure head h [m H_2O] $= \frac{\text{capillary pressure } p_c\text{[Pa]}}{\rho^{FR}\ \text{[kg m}^{-3}\text{]}\ g\ \text{[m s}^{-2}\text{]}}$ $\Rightarrow$ 1 [cm H_2O] = 100 [Pa]

$\alpha_{d/w}$ [Pa] $= \frac{1}{10\ g\ \text{[m s}^{-2}\text{]}\ h_{gd/gw}\ \text{[cm]}}$

prediction of the MWC from the MDC have been already determined in [7] and further material parameters necessary for the calculation of the acoustic properties have been specified by others before (e.g. in [8]). The material properties of Del Monte sand filled by an air-water mixture are summarized in Table 1.

Since the irreducible saturation is very small nearly the whole range of initial saturations $0.01 \leq S_0 \leq 1$ has been studied. The porosity of Del Monte sand is given in [8] by $n_0 = 0.2975$. The authors refer to measurements of Liakopoulos. Because the values for the MDC also were measured by him (see Figure 4) this value is also used here even if in the literature more plausible bigger values between 34.5% and 37% are mentioned. Also the Poisson ratio of 0.4 seems rather high and the solid grain density of 2000 kg m^{-3} rather low (compared to pure sand (mS) classified in the German standard DIN 4220 and studied in [3]). The rather low value for the water conductivity follows from the small value for the porosity. The value of the shear modulus has been estimated according to experiences gained on the study of some sands in [3].

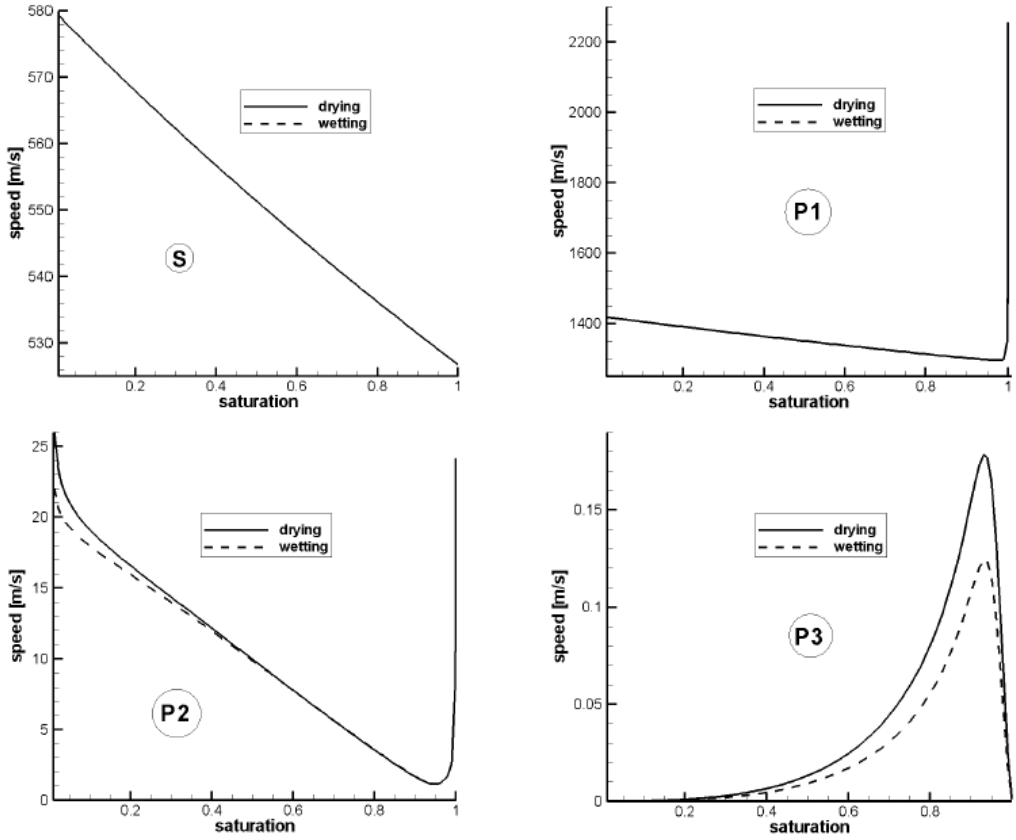

Figure 5: Phase speeds of the transversal wave S and the three longitudinal waves $P1$, $P2$ and $P3$ in dependence on the initial saturation S_0 using the parameters of the MDC (solid lines) and MWC (dashed lines); ($\omega = 1000$ Hz).

Exemplarily, the dependence of the phase speeds on the saturation is illustrated in Figure 5 for both MDC and MWC data of Del Monte sand filled by an air-water mixture. The wave propagation analysis predicts the existence of four sound waves: one transversal wave S and three compressional waves $P1$, $P2$ and $P3$. The $P1$-wave is mainly driven by the skeleton. The $P2$-wave shows a similar behavior to the sound wave in suspensions: its speed has a deep minimum in dependence on the saturation. The $P3$-wave only exists if at least two immiscible pore fluids occur. Its speed is attributed to the capillary pressure between the pore fluids.

In order to obtain the results illustrated in Figure 5 the frequency is chosen to be 1000 Hz. This is a typical value for geophysical applications. The results imply that – at least for the example of Del Monte sand filled with an air-water mixture – the influence of the hysteresis is very small.

An influence of the application of either drying or wetting data is noticeable most easily for the $P3$ wave. The maximum of the speed is bigger for drying than for wetting. Also for

the $P2$-wave a difference becomes evident. For small values of the saturation the wetting speeds are smaller than the drying speeds. However, these observations most likely do not have any practical bearing. Both the $P2$- and $P3$-waves, which are effected by the existence of the fluid and the gas, are strongly damped. For the $P3$-wave the attenuation is so high that an observation of this wave in the field may be nearly impossible.

The attenuations of the waves which are not presented here (see [2]) show in the range of low initial saturations (approximately 0-50%) also a small influence for $P1$-waves. This is a range of initial saturations which appears in arid regions. In such regions special measuring techniques are necessary because the capillary pressure or suction is extremely high. As pointed out above also the theoretical results show that the region of high capillary pressures must be attached an important bearing in the differentiation between wetting and drying.

As could be expected, the shear wave which is mainly affected by the shear modulus, the compressibility modulus and the mass density of the solid, is unconcerned of whether drying or wetting data are used. In contrast, the propagation of the $P3$-wave is influenced in the whole range of initial saturations. This could be expected because this wave arises only due to the capillary pressure or surface tension between the two pore fluids and this is different for drying and wetting for different saturations.

4 CONCLUSIONS

In this work the phenomenon of hysteresis in the capillary pressure in partially saturated soils, i.e. different drying and wetting curves for certain degrees of saturation, has been addressed. Two modeling approaches have been introduced. A mathematical model using a Preisach operator and a linear continuum model. Final aim is to construct a model with hysteresis operator which is able to describe wave propagation processes. Both presented models do not completely match this goal. The first contains an operator but is parabolic and thus not suitable to describe wave propagation. The second one is hyperbolic but does not contain an operator so that drying and wetting data have to be employed separately. Nevertheless the wave analysis has been carried out by means of the latter model for the example of Del Monte sand filled by an air-water mixture. Four waves appear: one transversal wave and three longitudinal waves. For the waves driven mainly by the skeleton it could be expected that the influence of the hysteresis in the capillary pressure curve is negligible or small. This is different from the expectations for the pore fluid driven waves. The numerical results exhibit a smaller influence than expected. This may have several reasons: firstly, the porosity of the studied sand has been chosen rather small, secondly, it may be not sufficient to investigate only one soil type, thirdly, the prediction of the main wetting curve should be proven by own experimental data. Therefore the measurement of the main drying and wetting curves of twelve different soil types studied in [3] has been requested in a laboratory and will be interpreted theoretically once available.

ACKNOWLEDGEMENT
Financial support as an Einstein Junior Fellow by the Einstein Foundation Berlin is highly appreciated.

REFERENCES

[1] Albers, B. Modeling the hysteretic behavior of the capillary pressure in partially saturated porous media - a review. Accepted for publication in *Acta Mechanica* (2014).

[2] Albers, B. Main drying and wetting curves of soils on measurements, prediction and influence on wave propagation, submitted to *Engineering Transactions* (2013).

[3] Albers, B. *Modeling and Numerical Analysis of Wave Propagation in Saturated and Partially Saturated Porous Media*. Habilitation thesis, Shaker Verlag, Aachen (2010).

[4] Bear, J. and Bachmat Y. *Introduction to Modeling of Transport Phenomena in Porous Media*. Kluwer Academic Publishers, Dordrecht (1991).

[5] Flynn, D. *Modelling theflow of water through multiphase porous media with the Preisach model*. PhD thesis, University College Cork (2008).

[6] Flynn, D., McNamara, H., O'Kane, J.P. and Pokrovskii, A. Application of the Preisach model to soil-moisture hysteresis. In *The Science of Hysteresis*, Vol. 3, M. Bertotti, Ed. Elsevier Science (2005), pp. 689.

[7] Haverkamp, R., Reggiani, P., Ross, P.J. and Parlange, J.-Y. Soil water hysteresis prediction model based on theory and geometric scaling. In *Environmental Mechanics, Water, Mass and Engergy Transfer in the Biosphere*, P.A.C. Raats, D. Smiles, A.W. Warrick, Ed. (2002) 213–246.

[8] Lewis, R.W. and Schrefler, B.A. *The finite element method in the static and dynamic deformation and consolidation of porous media*. Wiley, Chichester (1998).

[9] Liakopoulos, A.C. Theoretical approach to the solution of the infiltration problem. *International Association of Scientific Hydrology* (1966) **11**(1):69–110.

[10] Parlange, J.-Y. Capillary hysteresis and the relationship between drying and wetting curves. *Water Resources Research* (1976) **12**(2):224–228.

[11] Preisach, F. Über die magnetische Nachwirkung. *Zeitschrift für Physik* (1935) **94**:277–302.

[12] Van Genuchten, M.T. A closed-form equation for predicting the hydraulic conductivity of unsaturated soils. *Soil Sci. Soc. Am. J.* (1980) **44**:892–898.